Hydrodynamic Models of Partner WECs

T4.3

Thomsen, Jonas Bjerg

Publication date:
2018

Document Version
Publisher's PDF, also known as Version of record

DEPARTMENT OF CIVIL ENGINEERING
AALBORG UNIVERSITY

Hydrodynamic Models of Partner WECs

T4.3

Jonas Bjerg Thomsen

ISSN 1901-726X
DCE Technical Report No. 246

Aalborg University
Department of Civil Engineering
Wave Energy Research Group

DCE Technical Report No. 246

Hydrodynamic Models of Partner WECs

T4.3

by

Jonas Bjerg Thomsen

June 2018

Scientific Publications at the Department of Civil Engineering

Technical Reports are published for timely dissemination of research results and scientific work carried out at the Department of Civil Engineering (DCE) at Aalborg University. This medium allows publication of more detailed explanations and results than typically allowed in scientific journals.

Technical Memoranda are produced to enable the preliminary dissemination of scientific work by the personnel of the DCE where such release is deemed to be appropriate. Documents of this kind may be incomplete or temporary versions of papers—or part of continuing work. This should be kept in mind when references are given to publications of this kind.

Contract Reports are produced to report scientific work carried out under contract. Publications of this kind contain confidential matter and are reserved for the sponsors and the DCE. Therefore, Contract Reports are generally not available for public circulation.

Lecture Notes contain material produced by the lecturers at the DCE for educational purposes. This may be scientific notes, lecture books, example problems or manuals for laboratory work, or computer programs developed at the DCE.

Theses are monograms or collections of papers published to report the scientific work carried out at the DCE to obtain a degree as either PhD or Doctor of Technology. The thesis is publicly available after the defence of the degree.

Latest News is published to enable rapid communication of information about scientific work carried out at the DCE. This includes the status of research projects, developments in the laboratories, information about collaborative work and recent research results.

Published 2018 by
Aalborg University
Department of Civil Engineering
Thomas Manns Vej 23
DK-9220 Aalborg Ø, Denmark

Printed in Aalborg at Aalborg University

ISSN 1901-726X
DCE Technical Report No. 246

Preface

This report describes the hydrodynamic models used for the four WECs in the *"Mooring Solutions for Large Wave Energy Converters"* project: Floating Power Plant, KNSwing, LEANCON Wave Energy and Wave Dragon. The report focusses on the hydrodynamic coefficients found from the open source BEM code Nemoh and lists relevant structural parameters to be used in future analysis. The report does not perform any dynamic analysis, but merely presents the parameters to be used.

The report is the outcome of Work Package 4, Task 4.3 of the project and was produced by Aalborg University.

For information regarding the report and project, please contact Jonas Bjerg Thomsen (jbt@civil.aau.dk).

Aalborg University, June 29, 2018

Contents

1 | Introduction

The present report is part of the Danish EUDP project *"Mooring Solutions for Large Wave Energy Converters"* (MSLWEC). The project aims at improving mooring solutions for WECs by applying standard design procedures, novel mooring solutions and materials and ensure the possibility of a certified mooring system by use of appropriate design tools. As part of the work, numerical models are applied, primarily considering boundary element method (BEM) codes. This report aims at providing the baseline for these models by presenting structural and hydrodynamic properties for the four WECs in the project. The devices are:

1. Floating Power Plant
2. KNSwing
3. LEANCON
4. Wave Dragon

The report is structured in six chapter including this Introduction. The following chapters describe the hydrodynamic models for each of the partner WECs. Each chapter follows a similar structure and can easily be read separately. The chapters merely presents structural parameters and the hydrodynamic coefficients found from the BEM code Nemoh [1], while no analysis of the response or results are performed. For description of work where the models are used see e.g. [2]. The final chapter make a coarse comparison of the results obtained from the devices in order to present potential differences between them.

The report is part of *"Work Package 4: Full Analysis"* in the MSLWEC project and covers part of *"Task 4.3: Full Dynamic Analysis of Final Mooring Solution Candidates."*

2 | Floating Power Plant

The Floating Power Plant P60 is a hybrid energy platform, utilizing energy absorption from both wind and waves. The device consists of a floating platform on which the wind turbine and the wave energy PTO is located. The energy absorption is based on the principle of wave activated bodies, cf. e.g. [3], through four pitching floaters. A smaller scale version of the P60 (a P37 device) has previously been tested offshore in Denmark, while the current P60 device is planned for deployment at the Belgian coast, cf. [4]. The device is designed to be moored with a turret mooring system, originally planned as catenary mooring chains. In recent research ([4, 5]), it was shown that synthetic lines were potential cost reduction drivers and these are the future focus of the P60 device. This report merely focuses on the structure and hydrodynamic parameters and not the mooring analysis. For more information on the mooring see e.g. [2].

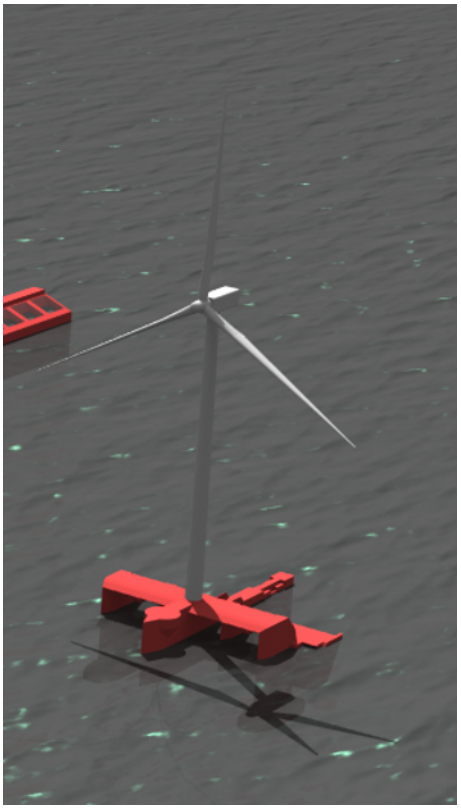

Fig. 2.1. Illustration of the Floating Power Plant P60 WEC.

2.1 Type of Analysis

The hydrodynamic response of the WEC can be obtained through different methods. The more sophisticated numerical models being e.g. CFD or SPH, while a linear BEM is often used due to its simplicity and time efficiency. This report considers only linear potential BEM methods and the open source code Nemoh [1].

Similarly, only extreme cases are considered where long waves are present and the dominant load regime is in the diffraction regime. At resonance frequencies and due to the long waves, quadratic drag contributions also becomes important to include in the numerical model. This will be described in a following section and has also been treated in [6].

In extreme cases, the wind turbine is parked and the floaters are ballasted so that their natural frequencies are outside the wave spectrum and the full structure moves as one solid.

In [7, 8], experimental tests of a simplified model of the P60 was described and the hydrodynamic model for this is compared to the present model for the actual P60 in order to illustrate differences.

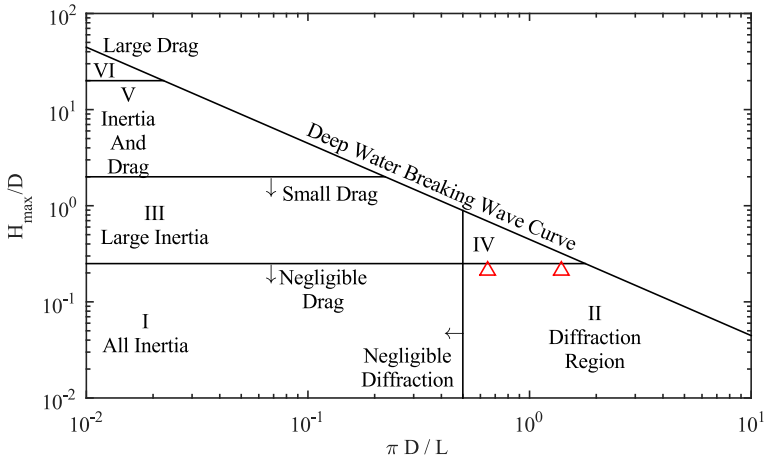

Fig. 2.2. Definition of the dominant force contributions for the P60 in the extreme sea states. Based on the diagram in [9]

2.2 Structure Specifications

The structure is a 60 m wide structure as illustrated in Fig. 2.1. The structural specifications of the full structure are presented in Table 2.1 in full-scale values. Only the geometry below SWL is considered in the BEM, and a panel mesh is constructed for analysis in Nemoh. The mesh is illustrated in Fig. 2.3 and has a total of 2310 panels.

Name	Unit	Value		
Structural Mass	[kg]	7,813,125		
Length	[m]	72.0		
Width	[m]	60.0		
Draught	[m]	8.3/17.7		
Centre of Gravity	[m]	x	y	z
		35.6	0.0	-5.8
Mass Moment of Inertia	$[\text{kg m}^2]$	x	y	z
wrt CoG	x	$2.06 \cdot 10^9$	0.0	0.0
	y	0.0	$2.37 \cdot 10^9$	0.0
	z	0.0	0.0	$3.56 \cdot 10^9$
Fairlead coordinate	[m]	x	y	z
wrt CoG		-26.4	0.0	-2.5

Table 2.1. Structural parameters used in the full dynamic analysis.

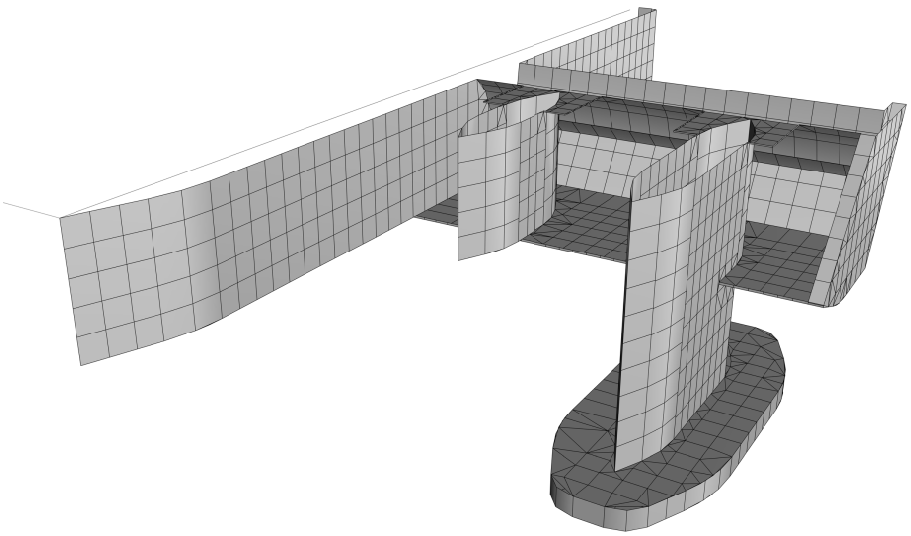

Fig. 2.3. Panel mesh used for hydrodynamic analysis in the BEM code Nemoh.

2.3 BEM Results

The results from the BEM model consist of the frequency dependent added mass and radiation damping coefficients together with the wave excitation and wave drift force

Hydrostatic Stiffness			
	Heave	Roll	Pitch
Heave	$9.48 \cdot 10^3$	0.0	$-7.85 \cdot 10^3$
Roll	0.0	$2.12 \cdot 10^6$	0.0
Pitch	$-7.85 \cdot 10^3$	0.0	$1.36 \cdot 10^6$

Table 2.2. Definitions of the hydrostatic stiffness of the structure.

coefficients. From these parameters, the RAOs are calculated. All results are plotted in Figure 2.4 - 2.7.

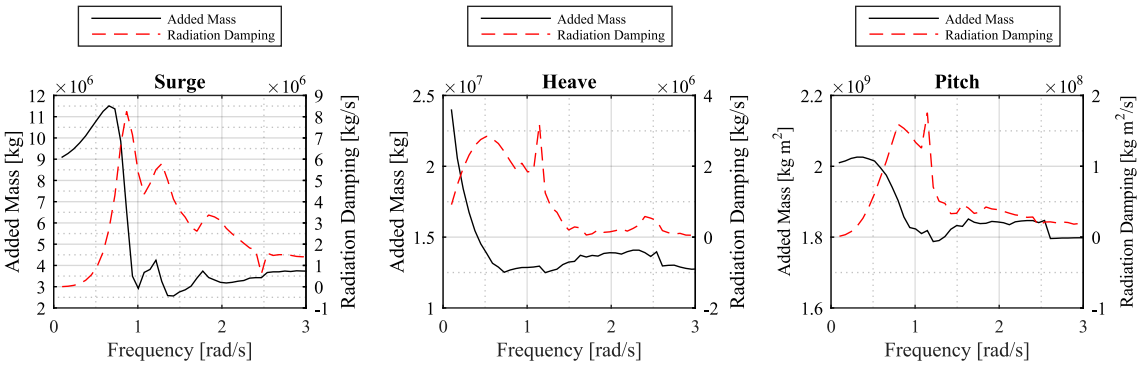

Fig. 2.4. Added mass and radiation damping coefficients for the surge, heave and pitch DoF. Note the different y-axes.

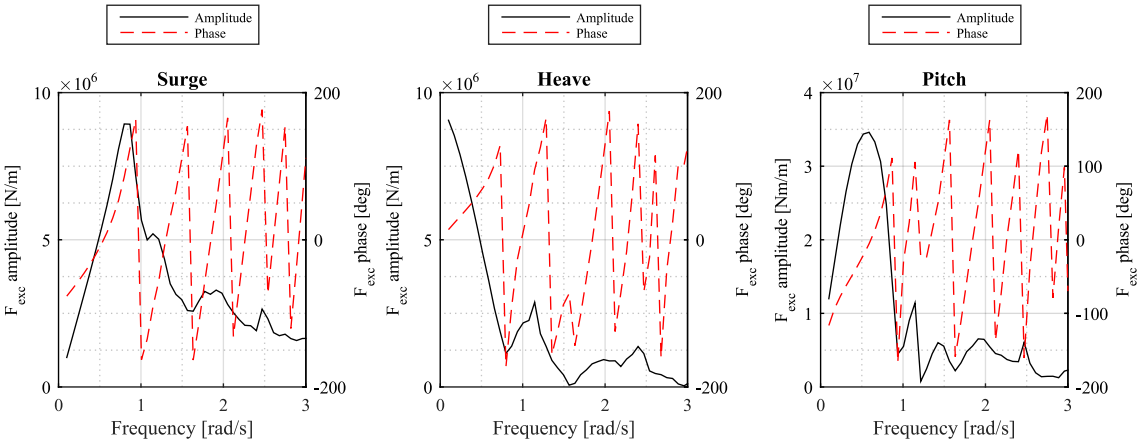

Fig. 2.5. Wave excitation force amplitudes and phases for surge, heave and pitch DoF. Note the different y-axes.

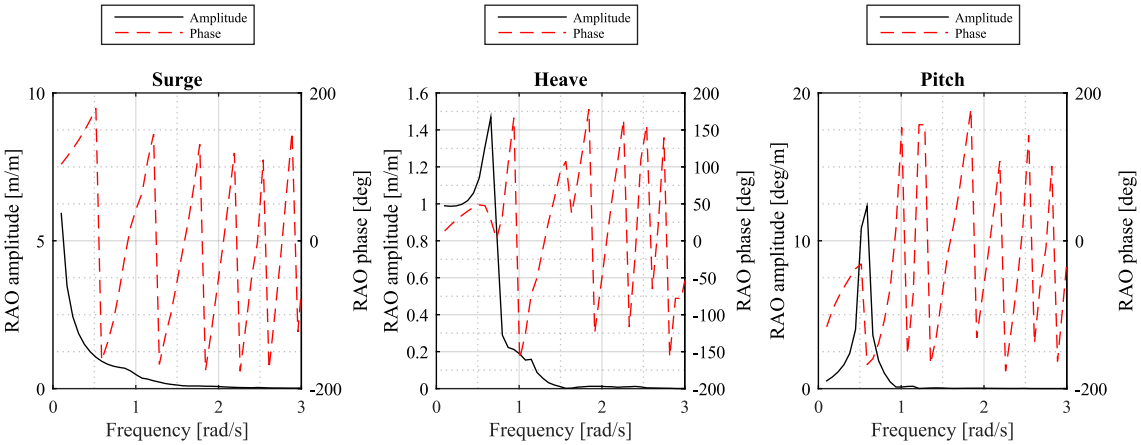

Fig. 2.6. Motion RAO amplitudes and phases for surge, heave and pitch DoF. Note the different y-axes.

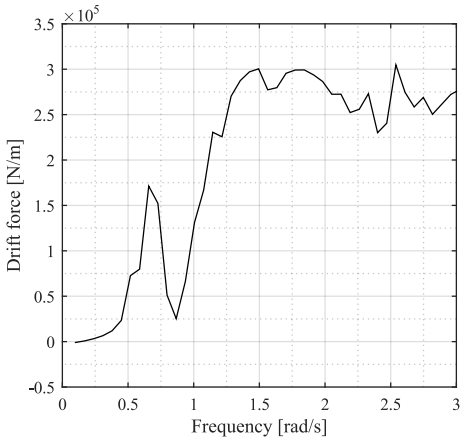

Fig. 2.7. The wave drift coefficients in the surge DoF.

2.4 Drag Element Approximation

The loads on the structure is not only composed of radiation/diffraction contributions, but also drag. This is most outspoken at extreme sea states where the wave length is long compared to the structure dimensions and when the motion peak frequencies are reached. As presented in [6], a simplified methodology can be applied to estimate drag coefficients and, thereby, utilize a hybrid numerical model that accounts for both diffraction, radiation and drag. The latter through Morison's Equation [10]. Similarly, a drag formulation is used to apply wind forces on the structure, for which reason, drag coefficients and areas are defined in Table 3.3. The simplified P60 model used to estimate coefficients is presented in Fig. 2.8.

Fig. 2.8. Illustration of the simplified geometry used for calculation of drag coefficients. The dark color resembles the geometry below the SWL, while the light grey color resembles geometry above.

DoF	Drag area	C_d	Load origin (z)
		Below SWL	
Surge	736 m^2	1.35	0.0 m
Heave	1580 m^2	1.30	0.0 m
Pitch	8.39·10^6 m^5	1.30	0.0 m
		Above SWL	
Foundation	173 m^2	1.14	10.0 m
Tower	291 m^2	1.10	53.4 m
Blades	150 m^2	0.01	95.3 m

Table 2.3. Drag force coefficients and areas for the P60.

2.5 Comparison with Experimental Model

In [7] and [6], a simplified model of the P60 was experimentally tested and in Fig. 2.11 - 2.14, the hydrodynamic parameters for each model is compared. It is clear that there is a significant difference between the two, due to difference in structure geometry, cf. Fig. 2.9.

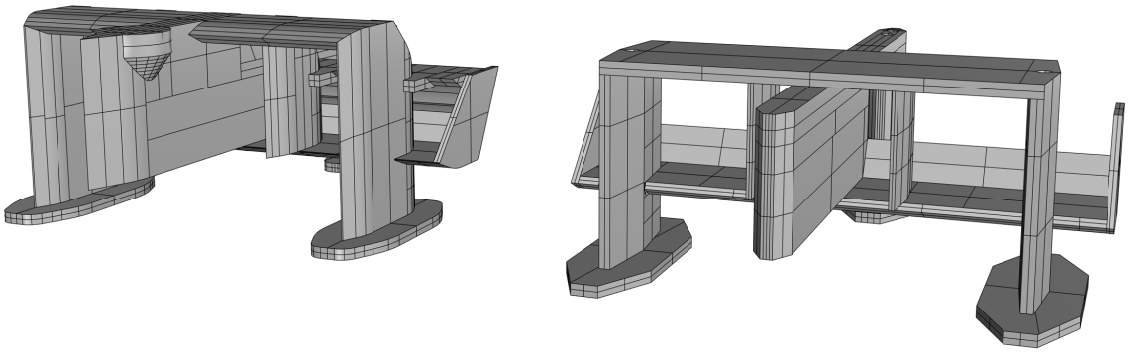

Fig. 2.9. Illustration of the P60 structure (left) and the simplified model used in the experimental work in [7] and [6].

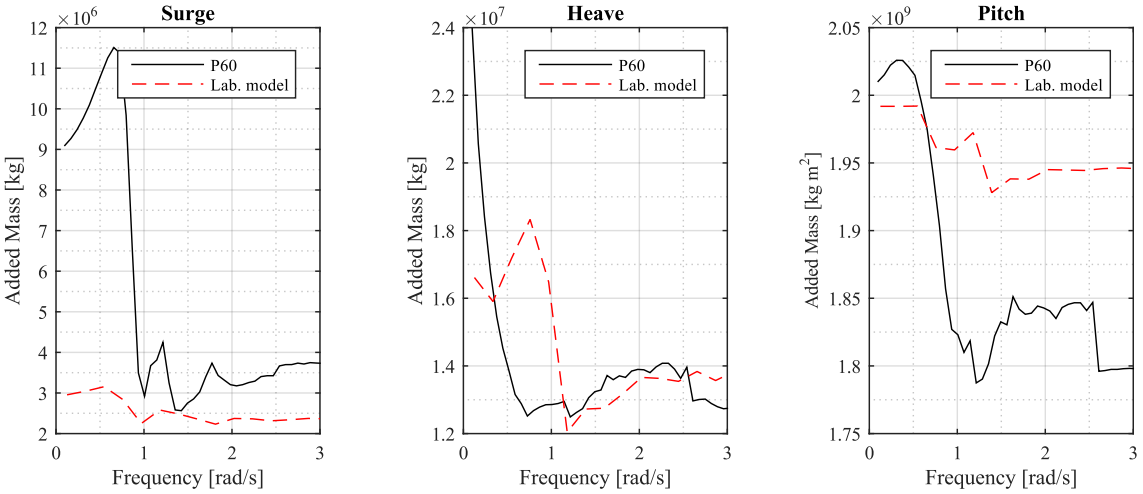

Fig. 2.10. Added mass and radiation damping coefficient for the surge, heave and pitch DoF. Note the different y-axes.

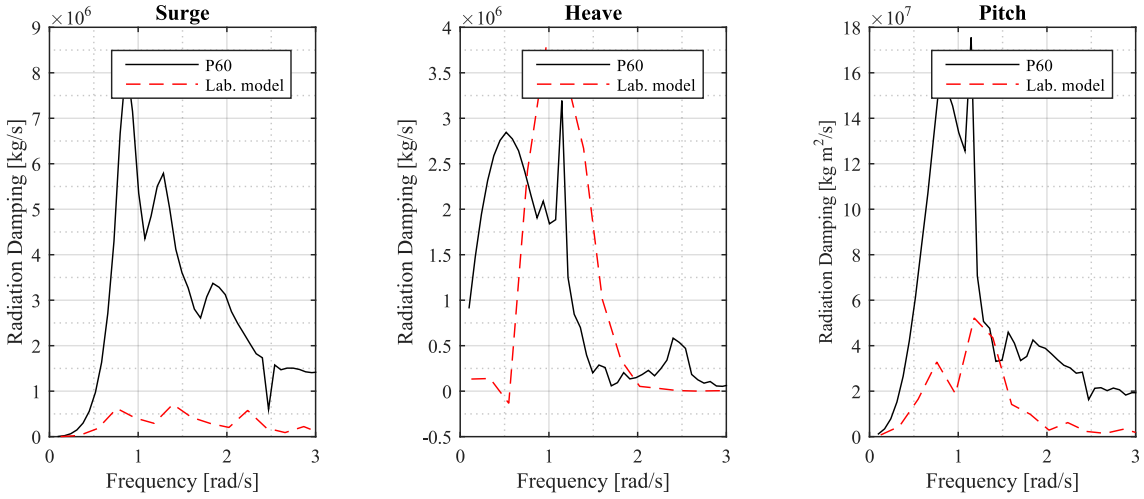

Fig. 2.11. Added mass and radiation damping coefficient for the surge, heave and pitch DoF. Note the different y-axes.

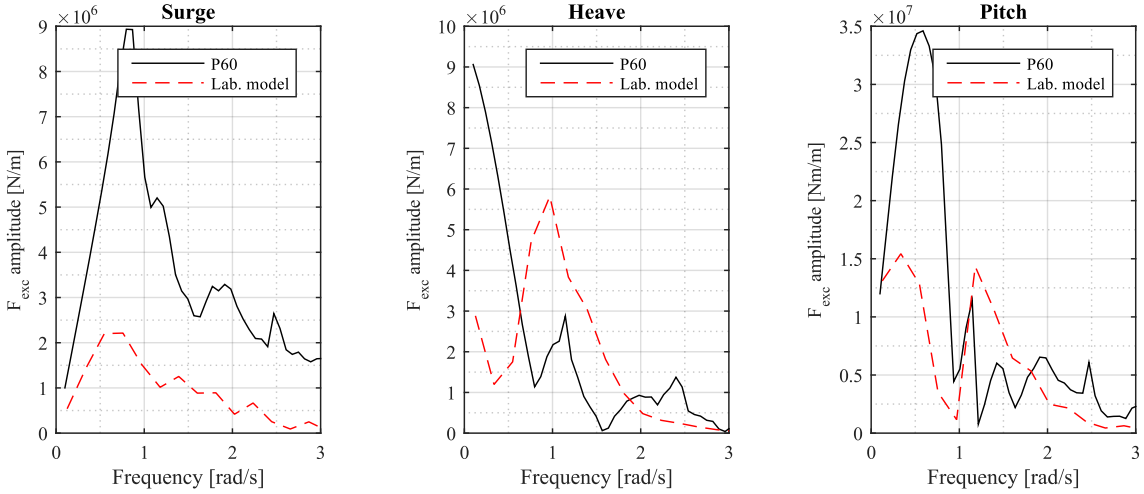

Fig. 2.12. Wave excitation force amplitude and phase for surge, heave and pitch DoF. Note the different y-axes.

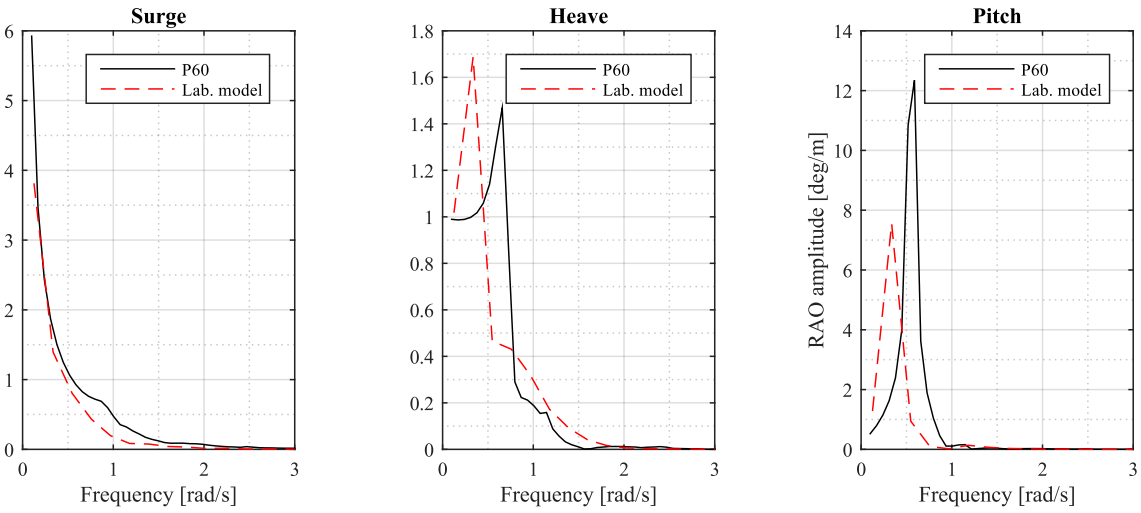

Fig. 2.13. Motion RAO amplitude and phase for surge, heave and pitch DoF. Note the different y-axes.

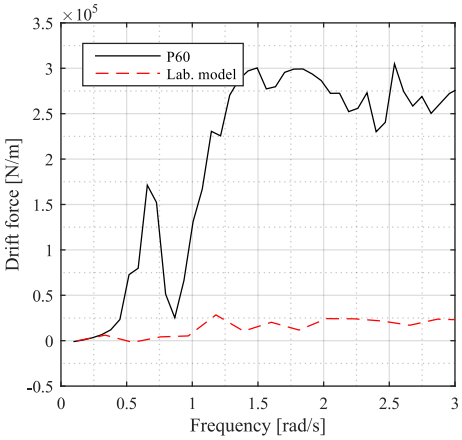

Fig. 2.14. The wave drift coefficient in the surge DoF.

It is evident that the absence of the floaters in the experimental model is resulting in a much smaller volume and hence, smaller loads, added mass and damping. Particularly the drift forces on the experimental model, where the water flows through it, results in much smaller loads compared to the actual P60, which has a much larger cross-sectional area. The results cannot directly be used to validate the results for the P60, but illustrate the difference between the simple model and the actual P60.

3 | KNSwing

The KNSwing is a WEC, using the concept of oscillating water columns for harvesting of the wave energy. The device is a ship-like structure with 20 OWC chambers on each side. The structure is planned for deployment in the Danish part of the North Sea and in full scale has a total length of 240 m. The structure is designed to be moored with a turret mooring system, and has so far been expected to be moored with synthetic nylon lines. In spite of being a part of the mooring project, this chapter will not deal with the mooring system, but only consider the structure and hydrodynamic modelling of it.

This chapter summarizes the results from the hydrodynamic modelling of the KNSwing and lists the parameters needed to construct a time domain model of the structure.

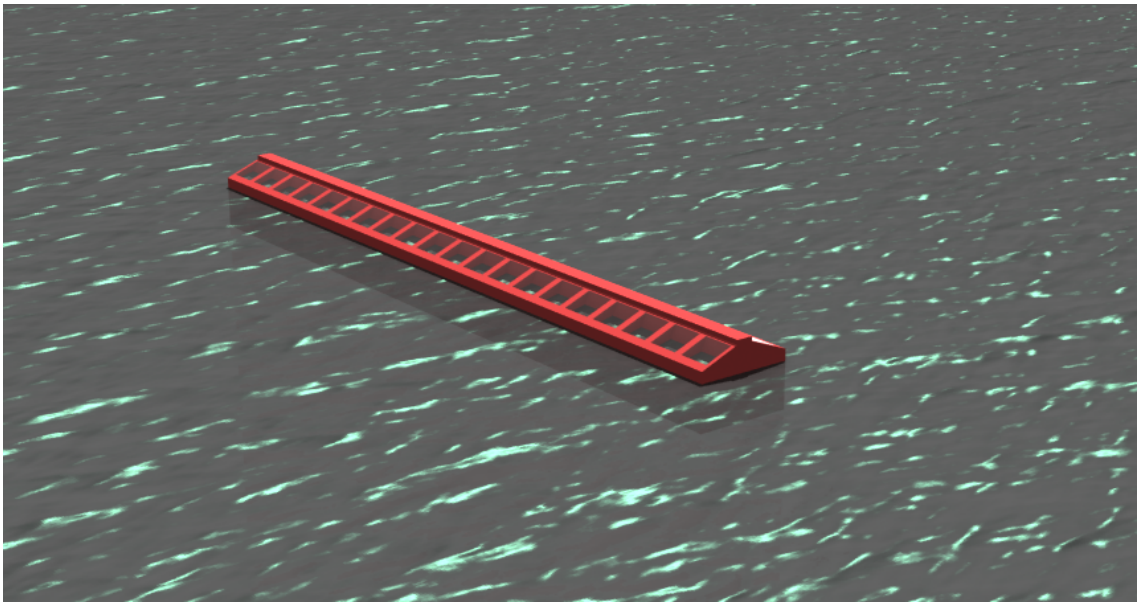

Fig. 3.1. Illustration of the KNSwing OWC WEC.

3.1 Type of Analysis

As described in previous chapters, the most sophisticated model of the hydrodynamic response of the WEC can be obtained by considering non-linear models like SPH/CFD, but this project is limited to the use of linear potential flow theory through the BEM using the open source code Nemoh [1].

This research project is limited to the ULS, hence extreme wave, wind and current conditions are assumed. In such a state, it is assumed that the PTO is disabled and, therefore, does not affect the response. In previous studies by [11] a hydrodynamic model was analysed in the BEM code WAMIT [12], with more detailed description of

the OWC chambers. The present studies uses the results from these to ensure validity of the constructed model, but does also use a limited number of experimental laboratory results to see that the numerical model provides similar results to these.

The dominant force regimes are in great extent determined by the structure size compared to the incoming wave length. For a structure like the KNSwing, the width of the structure is not significant in relation to the extreme waves and drag/inertia might be more dominant than diffraction/radiation, which is calculated in the BEM model. Considering the force regimes defined by [9] and plotted in Fig. 3.2 for the outer limits of the extreme sea states, it is clear that diffraction/radiation is indeed not the most dominant load contributions. It is, therefore, necessary to include other contributions, which is done by including a drag element as described later in this chapter.

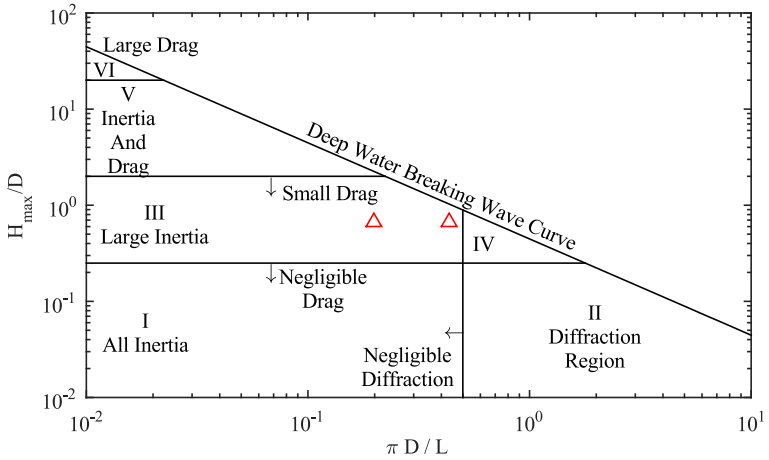

Fig. 3.2. Definition of the dominant force contributions for the KNSwing in the extreme sea states.

3.2 Structure Specifications

The WEC is a 240 m long ship-like structure as illustrated in Fig. 3.1. The structural specifications that are considered relevant for the hydrodynamic analysis are listed in Table 3.1 in full-scale values. All parameters are defined in previous work, but are relevant to consider when defining the numerical model. Only the geometry below the SWL is considered, and it is constructed by a panel mesh for use in the Nemoh code. For this project, the investigated mesh is illustrated in Fig. 3.3, with a total number of 2980 panels which was found feasible for the BEM model.

Name	**Unit**	**Value**		
Structural Mass	[kg]	44,748,800		
Length	[m]	240.0		
Width	[m]	28.0		
Draught	[m]	13.2		
Centre of Gravity	[m]	x	y	z
		0.0	0.0	-3.6
Mass Moment of Inertia	$[\text{kg m}^2]$	x	y	z
wrt CoG	x	$2.86 \cdot 10^9$	0.0	0.0
	y	0.0	$2.15 \cdot 10^{11}$	0.0
	z	0.0	0.0	$2.15 \cdot 10^{11}$
Fairlead coordinate	[m]	x	y	z
wrt CoG		-120.0	0.0	-13.2

Table 3.1. Structural parameters used in the full dynamic analysis.

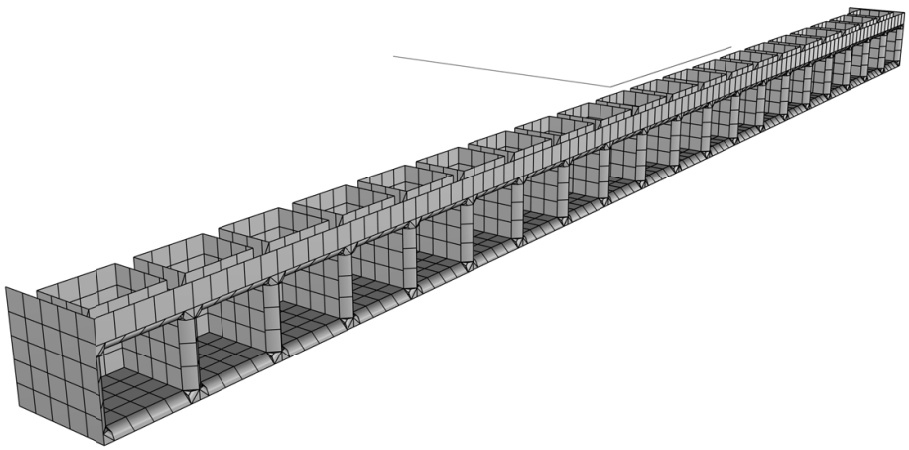

Fig. 3.3. Panel mesh used for hydrodynamic analysis in the BEM code Nemoh. Note the location of the co-ordinate system.

Hydrostatic Stiffness			
	Heave	Roll	Pitch
Heave	$35.9 \cdot 10^3$ kN/m	0.0	0.0
Roll	0.0	$1.03 \cdot 10^6$ kNm/rad	0.0
Pitch	0.0	0.0	$171.0 \cdot 10^6$ kNm/rad

Table 3.2. Definition of the hydrostatic stiffness of the structure.

3.3 BEM Results

The results from the BEM model consist of the frequency dependent added mass and radiation damping coefficients, together with the wave excitation and wave drift force coefficients. From these parameters, the RAOs are calculated. All results are plotted in Figure 3.4 - 3.7.

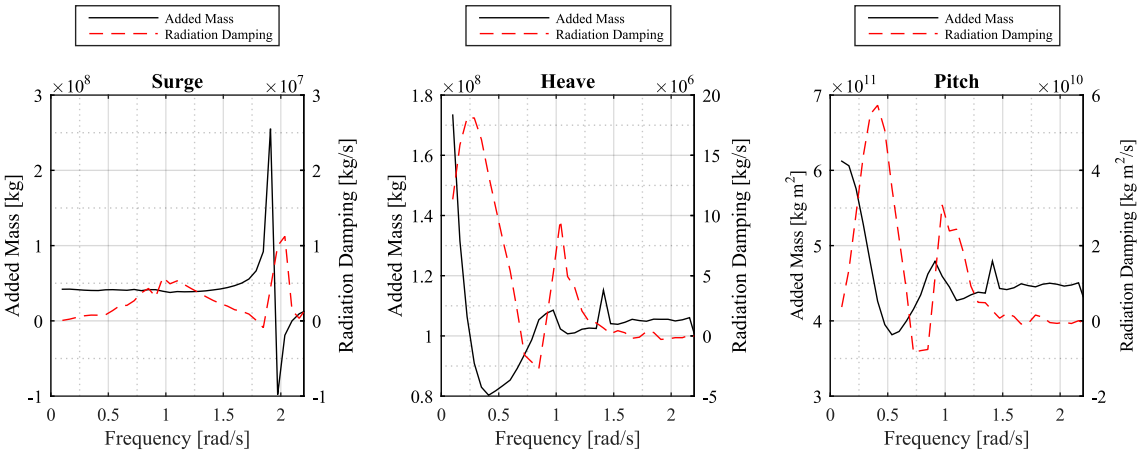

Fig. 3.4. Added mass and radiation damping coefficients for the surge, heave and pitch DoF. Note the different y-axes.

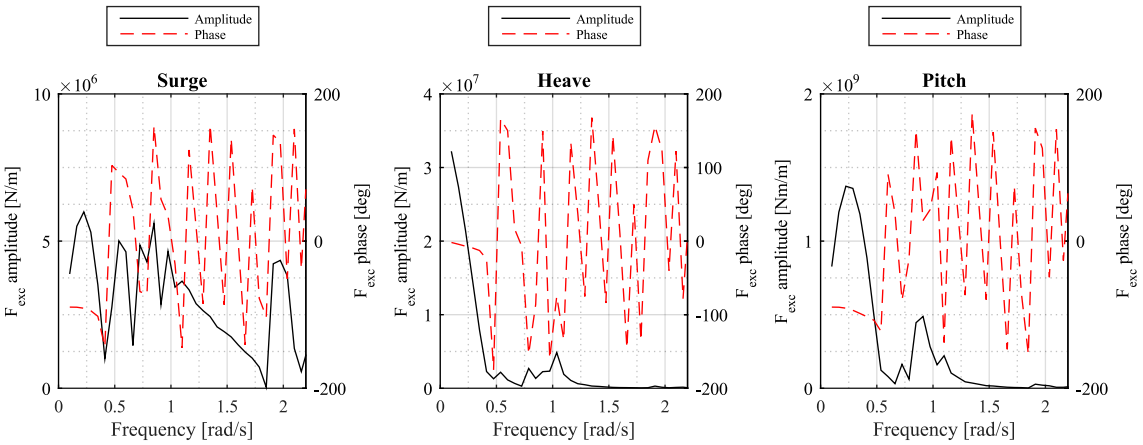

Fig. 3.5. Wave excitation force amplitudes and phases for surge, heave and pitch DoF. Note the different y-axes.

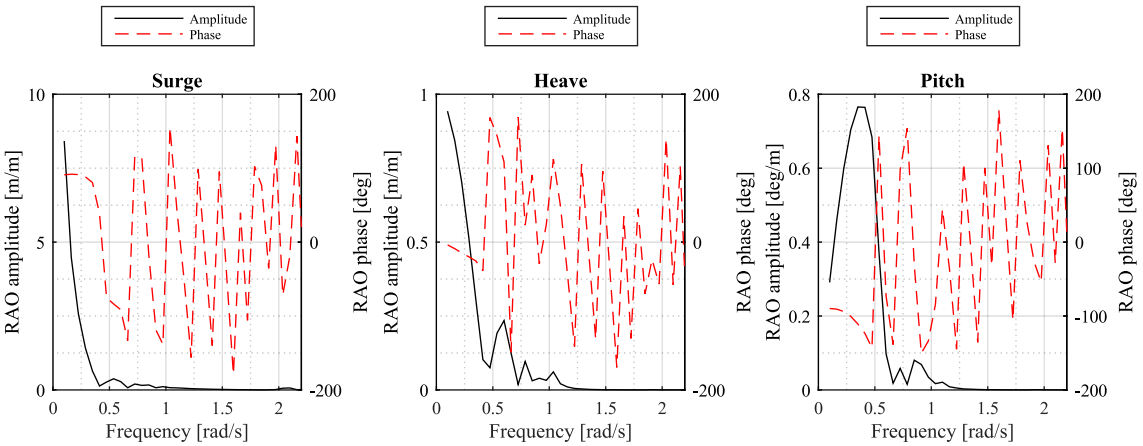

Fig. 3.6. Motion RAO amplitudes and phases for surge, heave and pitch DoF. Note the different y-axes.

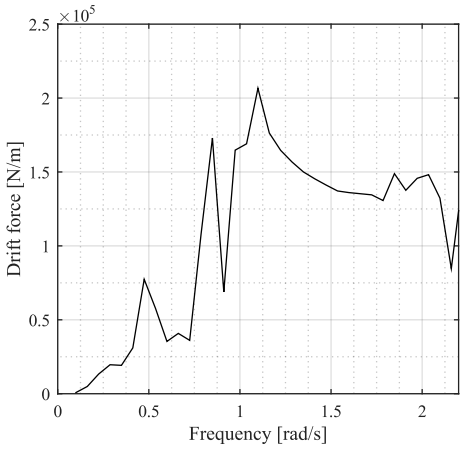

Fig. 3.7. The wave drift coefficients in the surge DoF.

3.4 Drag Element Approximations

As previously described, the KNSwing is not only exposed to radiation/diffraction loads, but also other contributions. In order to include that in future time domain simulations, it is necessary to define drag coefficients. In order to estimate these, a simplified geometry has been assumed, cf. Fig. 3.8, where the structure is composed of a rectangular box. Here, the OWC chambers and their influence on the drag is not included. Based on [13], the coefficients for the structure above and below SWL have been defined, and are listed in Table 3.3. Coefficients and areas have been defined for both surge, heave and pitch. The pitch drag moment coefficient has been found by considering the moment arms and drag forces.

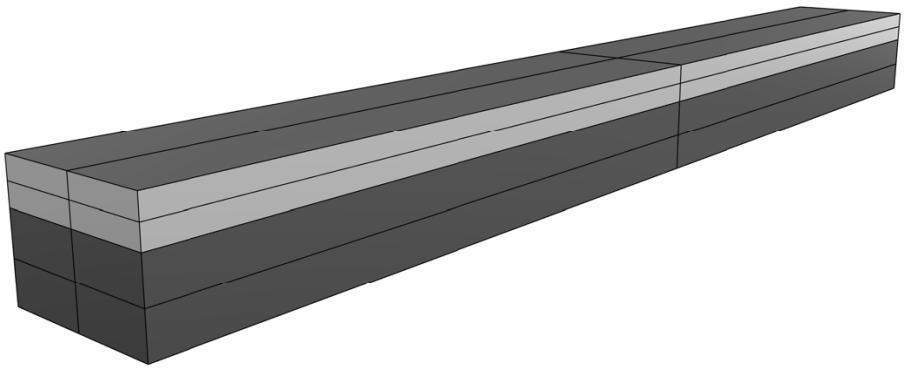

Fig. 3.8. Illustration of the simplified geometry used for calculation of drag coefficients. The dark color resembles the geometry below the SWL, while the light grey color resembles geomtry above.

DoF	Drag area	C_d	Load origin (z)
	Below SWL		
Surge	370 m^2	0.8	-3.0 m
Heave	6720 m^2	1.3	0.0 m
Pitch	$1.45 \cdot 10^9$ m^5	1.3	0.0 m
	Above SWL		
Surge	173 m^2	0.8	6.9 m

Table 3.3. Drag force coefficients and areas for the KNSwing.

3.5 Validation of Results

The procedure for calculation of hydrodynamic coefficients and definition of drag force coefficients follows a procedure, which has been validated comprehensively in the project. The work considered another structure and used a database of experimental results to investigate the potential error.

In order to ensure that this method provides similar results for the KNSwing and can be used in the full dynamic analysis, the found coefficients are compared to results from another numerical model [11]. Later, a simple OrcaFlex [14] model is constructed and compared to experimental results from a test campaign conducted in Portaferry, Ireland.

3.5.1 Comparison with Existing Models

In [11], a hydrodynamic model of the KNSwing was constructed. The added mass, damping and wave excitation forces from this model is plotted against the present model in Fig. 3.9-3.11. Reasonable agreement is seen between the two models. In the model by [11], a very distinct peak is seen, which does not appear as outspoken in the present model. It is observable in the surge added mass, for instance, but with a slight offset in the frequency and with a smaller amplitude.

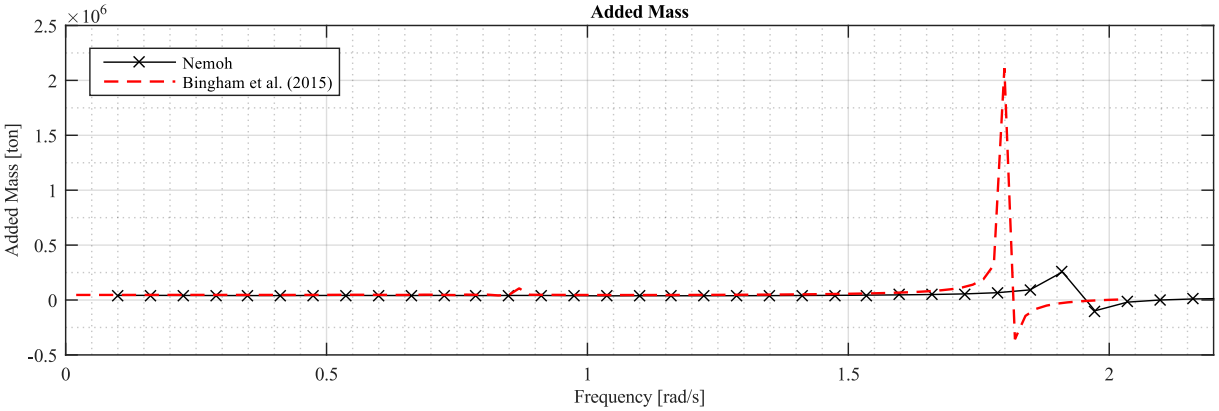

Fig. 3.9. Comparison of added mass found from the present BEM model and the results from [11].

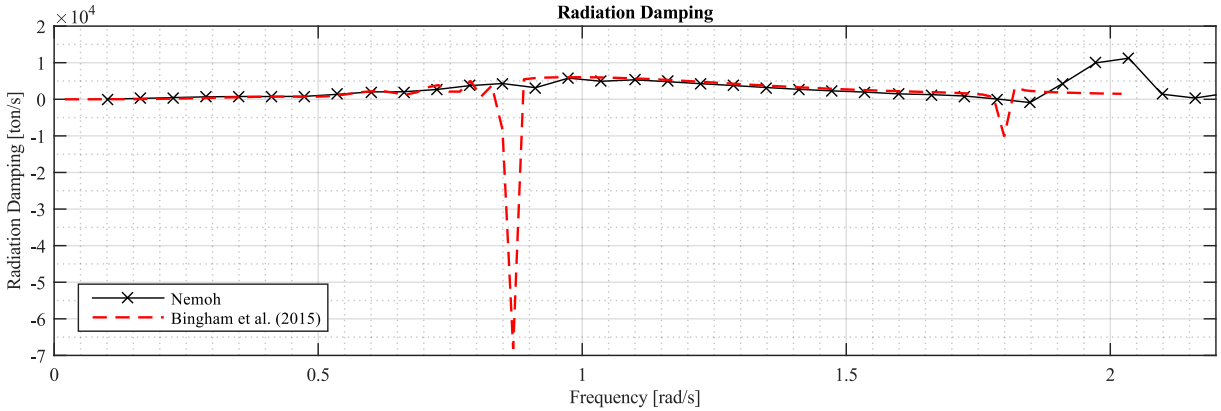

Fig. 3.10. Comparison of radiation damping found from the present BEM model and the results from [11].

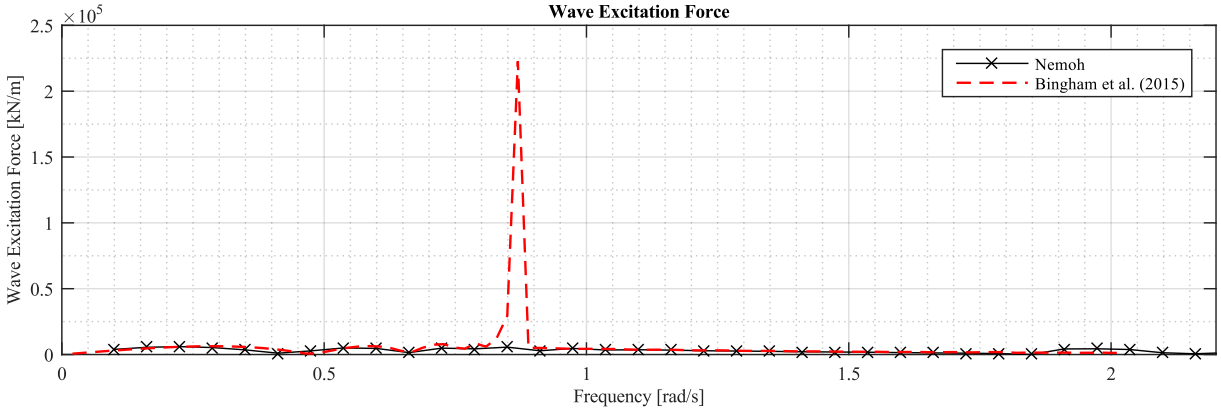

Fig. 3.11. Comparison of excitation forces found from the present BEM model and the results from [11].

3.5.2 Comparison with Experimental Results

In order to ensure that the numerical model provides satisfying results, a time domain model was constructed in OrcaFlex which resembled the set-up used in a test campaign conducted in Portaferry, Ireland. The set-up consisted of a 1:80 scale device, moored with three synthetic lines.

Seven sea states were selected and used for this simple validation. The line tension in one of the front lines were used as basis for comparison. The seven sea states are listed in Table 3.4, and the relative errors between tensions from numerical model and experiments are illustrated in Figure 3.12.

#	Sign. Wave Height H_s [m]	Wave Period T_z [s]
1	3.20	7.00
2	6.56	9.10
3	8.32	10.40
4	12.24	12.30
5	12.00	10.20
6	12.48	11.30
7	9.84	8.50

Table 3.4. Full-scale values of the sea states tested in the experiments and numerical model.

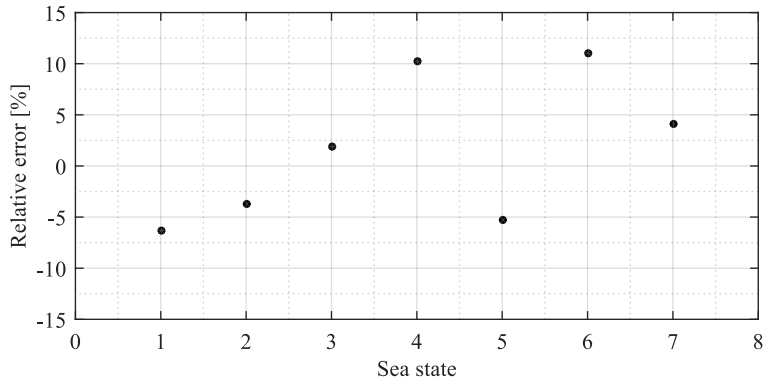

Fig. 3.12. Relative error between tensions found in experiments and numerical model for each of the sea states defined in Table 3.4.

As seen in Fig. 3.12, a relative small error is obtained with an absolute maximum of around 11%. This corresponds well with the tendency found from previous validations and use of same procedure [6]. Due to this, it as assumed that the model can be used in further initial analysis of the KNSwing and particularly the mooring system. Obviously, in a final design the experiments can be used to optimize the model further and ensure even smaller deviation between nature and model, but for an initial investigation, this error is found acceptable.

4 | LEANCON

The LEANCON WEC uses the OWC principle for absorption of the incoming wave energy, and is illustrated in Fig. 4.1. The structure is characterized by its low weight and V-shape structure. The structure is planned for deployment at the Danish part of the North Sea, but will prior by deployed at the DanWEC test facility in a scale 1:2. This report deals with this scale.

The WEC has been undergoing small-scale tests at Aalborg University, and by the end of 2015, it was deployed in a scale 1:10 at the offshore test facility at Nissum Bredning, Denmark. A mooring system has previously been proposed for the LEANCON, named SEBAS (Slacked Elastic Buoyancy Anchoring System), but this will not be treated in this report. For full dynamic analysis of the mooring system, the reader is referred to later reports. This chapter deals with the un-moored hydrodynamic modelling of the structure and provides all the necessary details to be used in the later full analysis.

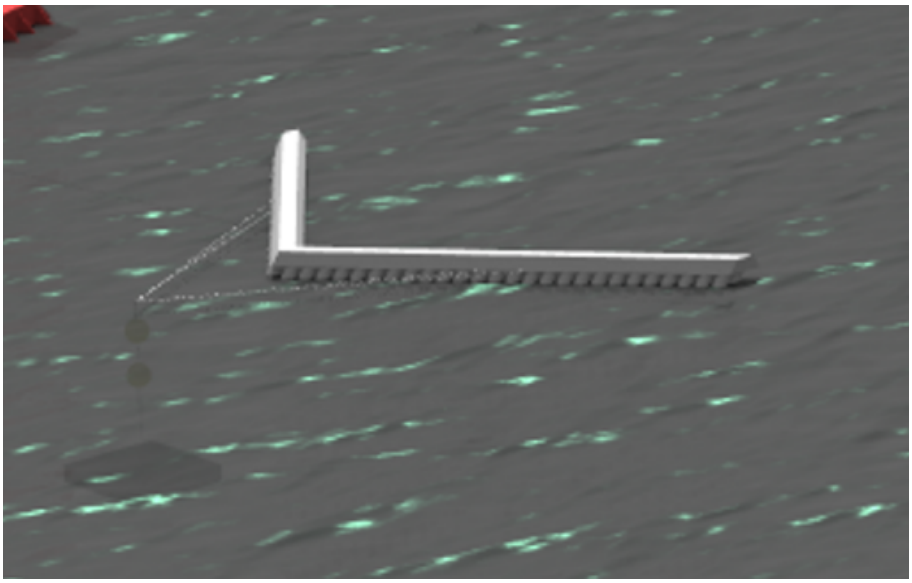

Fig. 4.1. Illustration of the LEANCON OWC WEC.

4.1 Type of Analysis

Several different models can be used in analysis of a floating structure; some more sophisticated than others. The level of included effects in the model is paid by computational time and in this project, only BEM is considered using the code Nemoh [1]. This model considers only the geometry below the SWL and might, therefore, induce some significant model errors, particularly as this project considers the ULS with extreme waves. The device is located in relatively shallow/intermediate water depths, and steep

waves can occur. This might provide underestimation of slamming loads on the device from breaking, and in general, the BEM model is out of its theoretical application area.

The LEANCON WEC is equipped with a storm protection mode, where the wave loads are attempted reduced. The device is capable of closing the OWC chambers and fill the structure with air, thereby increase buoyancy and decrease the draught. This mode is the objective of this study.

The LEANCON device is a relatively large structure, and it can be expected that the diffraction/radiation forces are the most dominant. Considering the load regimes as defined by [9] and plotted in Fig. 4.2 for the LEANCON and the extreme events, this assumptions seems correct. However, considering just the individual OWC tubes (cf. Fig. 4.3) in the extreme waves, drag loads might also become considerable.

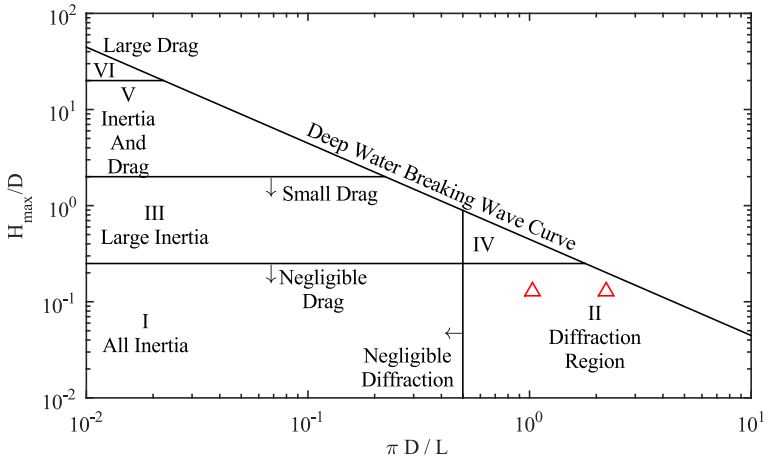

Fig. 4.2. Definition of the dominant force contributions for the LEANCON in the extreme sea states.

4.2 Structure Specifications

The WEC is a V-shaped structure as illustrated in Fig. 4.1. The parameters needed in the dynamic analysis are all listed in Table 4.1. Only the geometry below the SWL is considered in the analysis, and the constructed panel mesh is illustrated in Fig. 4.3, with a total number of 1664 panels.

Name	**Unit**	**Value**		
Structural Mass	[kg]		187,500	
Length	[m]		59.0	
Width	[m]		121.5	
Draught	[m]		1.25	
Centre of Gravity	[m]	x	y	z
		27.8	0	2.8
Mass Moment of Inertia	$[\text{kg m}^2]$	x	y	z
wrt CoG	x	$2.29 \cdot 10^8$	0	0
	y	0	$4.19 \cdot 10^7$	0
	z	0	0	$2.70 \cdot 10^8$
Fairlead coordinate	[m]	x	y	z
wrt CoG		-0.04	34.0	0.0
		-3.9	29.4	0.0
		-0.04	-34.0	0.0
		-3.9	-29.4	0.0

Table 4.1. Structural parameters used in the full dynamic analysis.

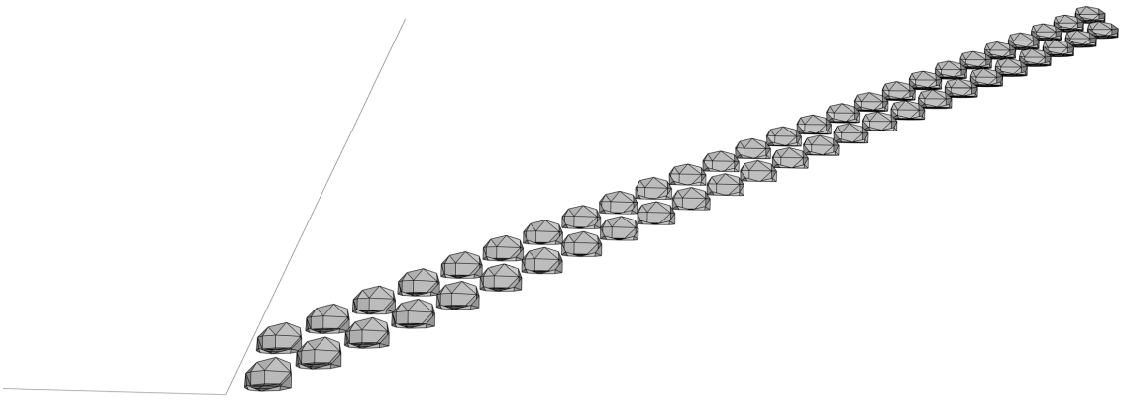

Fig. 4.3. Panel mesh used for the hydrodynamic analysis in the BEM code Nemoh.

4.3 BEM Results

The results from the BEM analysis is presented in the following figures. The presented values cover the radiation damping, added mass, wave excitation force amplitudes and phases, motion RAO amplitudes and phases, and the calculated drift force coefficients.

Hydrostatic Stiffness			
	Heave	Roll	Pitch
Heave	$5.25 \cdot 10^3$	0.0	$0.57 \cdot 10^3$
Roll	0.0	$6.34 \cdot 10^6$	0.0
Pitch	$-7.85 \cdot 10^3$	0.0	$1.12 \cdot 10^6$

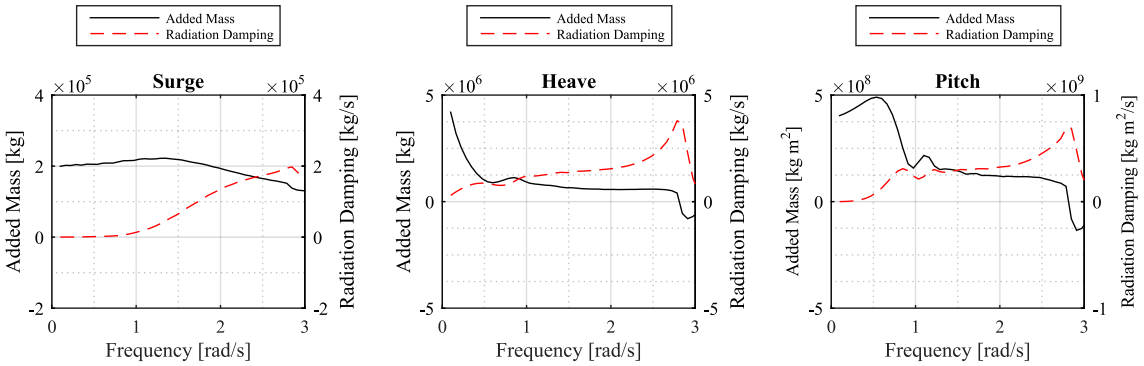

Fig. 4.4. Added mass and radiation damping coefficients for the surge, heave and pitch DoF. Note the different y-axes.

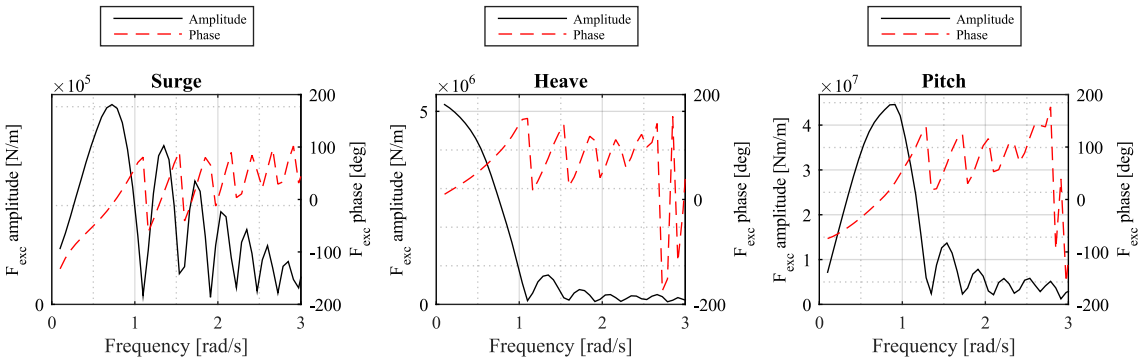

Fig. 4.5. Wave excitation force amplitudes and phases for surge, heave and pitch DoF. Note the different y-axes.

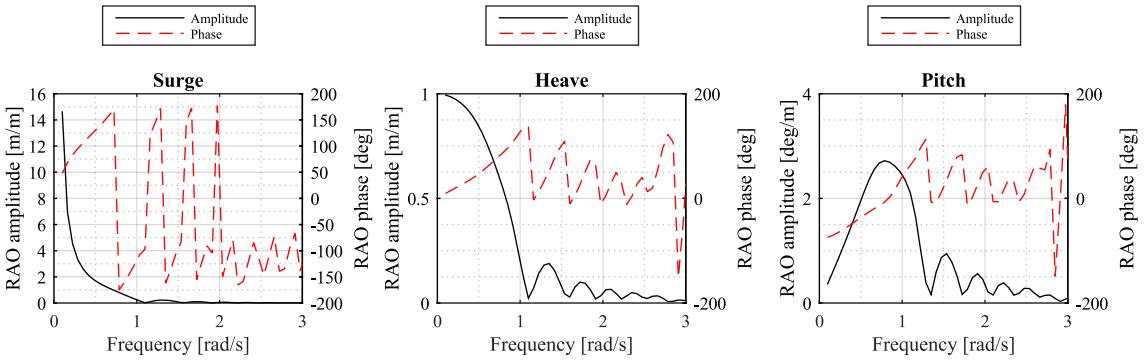

Fig. 4.6. Motion RAO amplitudes and phases for surge, heave and pitch DoF. Note the different y-axes.

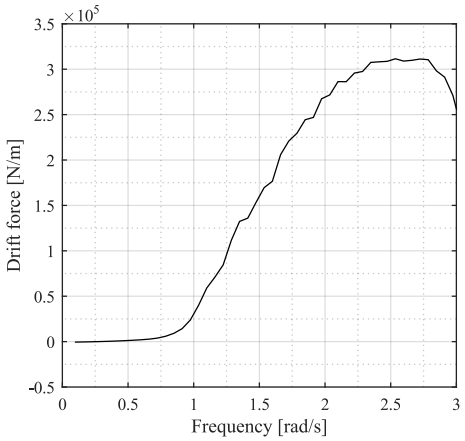

Fig. 4.7. The wave drift coefficients in the surge DoF.

4.4 Drag Element Approximations

In order to account for the other load contributions on the device, a drag element should be added to the model. This is done by defining drag areas and drag moment areas, together with the corresponding drag and drag moment coefficients. The coefficients need to be found either experimentally or by e.g. CFD in order to get as accurate an estimation as possible. In this project, neither of these are possible and, therefore, the values are estimated from a simplified geometry as illustrated in Fig. 4.8 and following the procedure in [6]. The shape of the WEC is approximated using rectangular shapes for which drag coefficients are defined in [13]. The drag moment coefficient is found by considering the force and moment arm. The values for both above and below SWL is defined in the following table. The values can be used in Morison's equation to evaluate drag loads.

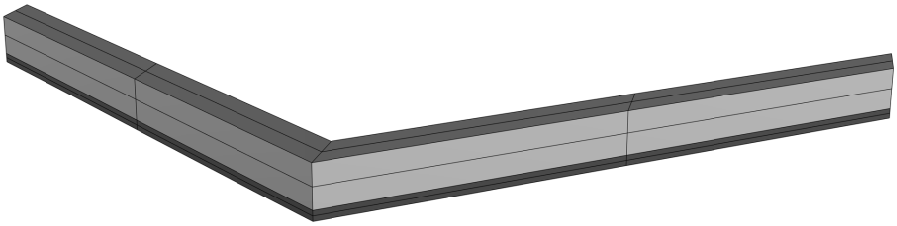

Fig. 4.8. Simplified geomtry of the LEANCON WEC used for estimation of the drag coefficients. The dark grey is the geometry below SWL, while the light grey is above.

DoF	**Drag area**	C_d	Load origin (z)
		Below SWL	
Surge	152 m^2	1.1	-3.4
Heave	889 m^2	1.3	0
Pitch	$1.96 \cdot 10^6$ m^5	1.3	0
		Above SWL	
Surge	645 m^2	1.1	0

5 | Wave Dragon

The Wave Dragon WEC (cf. Fig. 5.1) utilizes the principle of overtopping in order to harvest the wave energy. The 1.5 MW device is planned for deployment at the wave energy test facility DanWEC at Hanstholm, Denmark.

Wave Dragon has by now been undergoing comprehensive testing in laboratory scale and in larger scale in offshore real sea tests. The current mooring system is planned to consist of a SPM buoy connected to the seabed through composite lines of nylon and chain. Other publications [2], present the optimization of this system, while this report only treats the hydrodynamic properties of the un-moored structure.

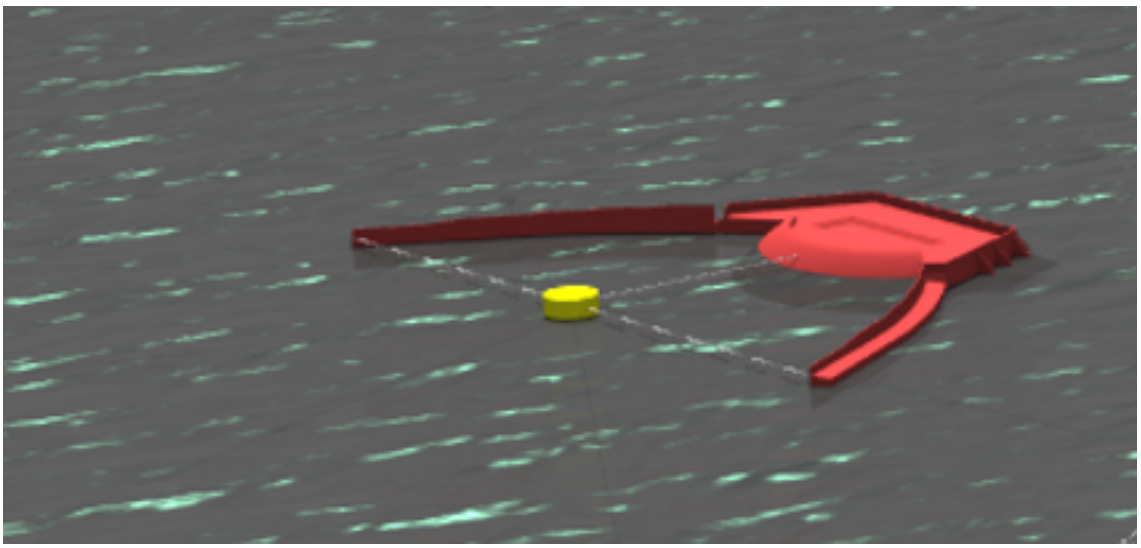

Fig. 5.1. Illustration of the Wave Dragon WEC.

5.1 Type of Analysis

Several methods are available for estimation of the structure response for a floating WEC. The most simple is the BEM, which invokes linear potential theory. However, this method induces a high level of inaccuracy for an overtopping WEC like the Wave Dragon. The method does not account for the water passing over the device, hence the loads are potentially extremely overestimated. Furthermore, the Wave Dragon is equipped with a storm protection mode which lowers the device below the SWL. In practice, this reduces the loads on the structure, but the increased displaced volume in the BEM calculations increases the loads. Consequently, using a BEM should be done with caution. More sophisticated models like CFD or SPH would provide more reliable results, but this is paid by much higher computational time. At present, this report continues to consider BEM results, while future research will focus on improving this method by using CFD

results to calibrate it.

The Wave Dragon is a large structure for which reason the diffraction/radiation loads can be expected to be dominant, cf. Fig. 5.2.

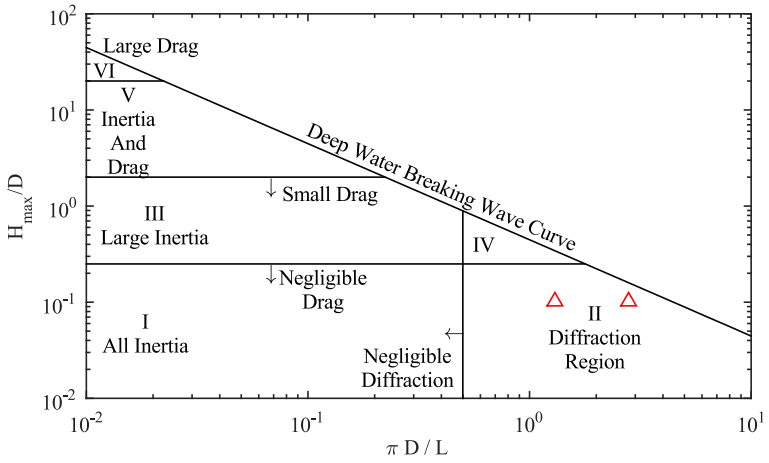

Fig. 5.2. Definition of the dominant force contributions for the Wave Dragon in the extreme sea states. Based on [9].

5.2 Structure Specifications

The structure consists of a main platform, cf. Fig. 5.1, with a reservoir for the overtopping. Furthermore, the device has two reflector arms which concentrate the wave energy towards the overtopping ramp. In the BEM, only the geometry below the SWL is considered (hence, the problem of load overestimation), and the constructed panel mesh is illustrated in Fig. 5.3. A total number of 2190 panels were used.

Name	**Unit**	**Value**		
Structural Mass	[kg]	7,000,000		
Length	[m]	72.0		
Width	[m]	60.0		
Centre of Gravity	[m]	x	y	z
		0	0.0	-3.38
Mass Moment of Inertia	$[\text{kg m}^2]$	x	y	z
wrt CoG	x	$9.17 \cdot 10^9$	0.0	0.0
	y	0.0	$2.15 \cdot 10^9$	0.0
	z	0.0	0.0	$1.12 \cdot 10^{10}$
Fairlead coordinate	[m]	x	y	z
wrt CoG		-20.0	0.0	1.3

Table 5.1. Structural parameters used in the full dynamic analysis.

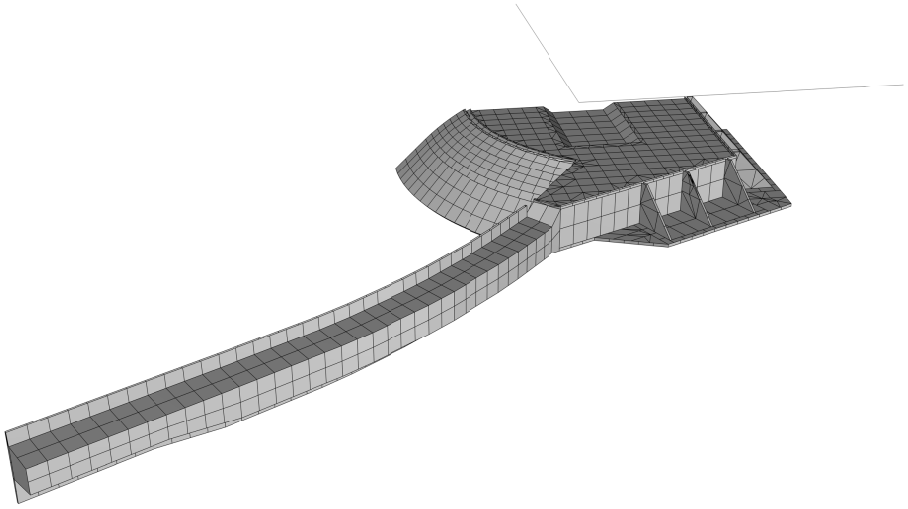

Fig. 5.3. Panel mesh used for hydrodynamic analysis in the BEM code Nemoh.

5.3 BEM Results

The results from the BEM analysis is presented in the following figures. The presented values cover the radiation damping, added mass, wave excitation force amplitudes and phases, motion RAO amplitudes and phases, and the calculated drift force coefficients.

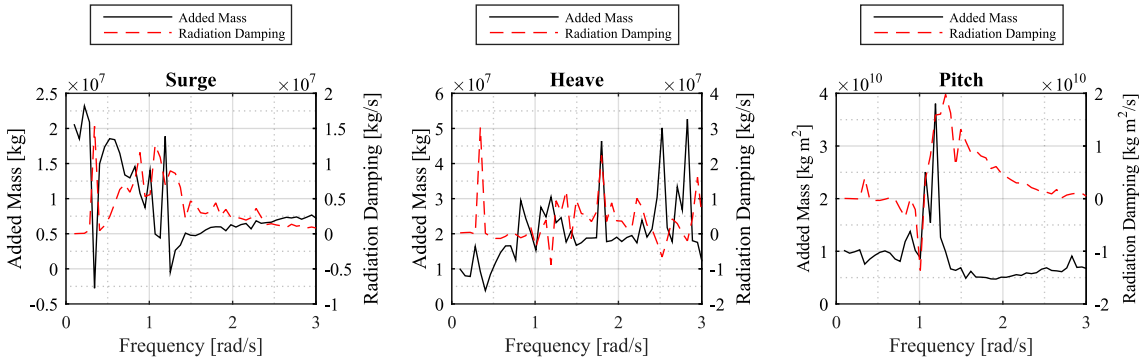

Fig. 5.4. Added mass and radiation damping coefficients for the surge, heave and pitch DoF. Note the different y-axes.

Hydrostatic Stiffness			
	Heave	Roll	Pitch
Heave	$1.19 \cdot 10^3$	0.0	$16.55 \cdot 10^3$
Roll	0.0	$1.36 \cdot 10^6$	0.0
Pitch	$16.55 \cdot 10^3$	0.0	$757.8 \cdot 10^3$

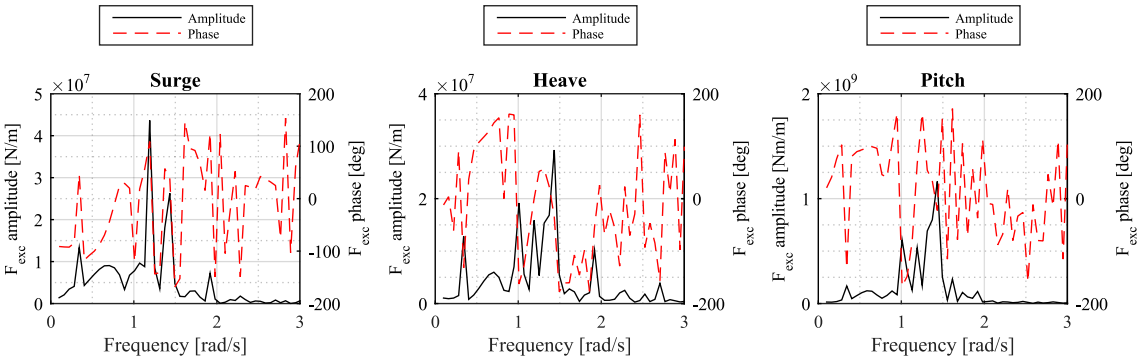

Fig. 5.5. Wave excitation force amplitudes and phases for surge, heave and pitch DoF. Note the different y-axes.

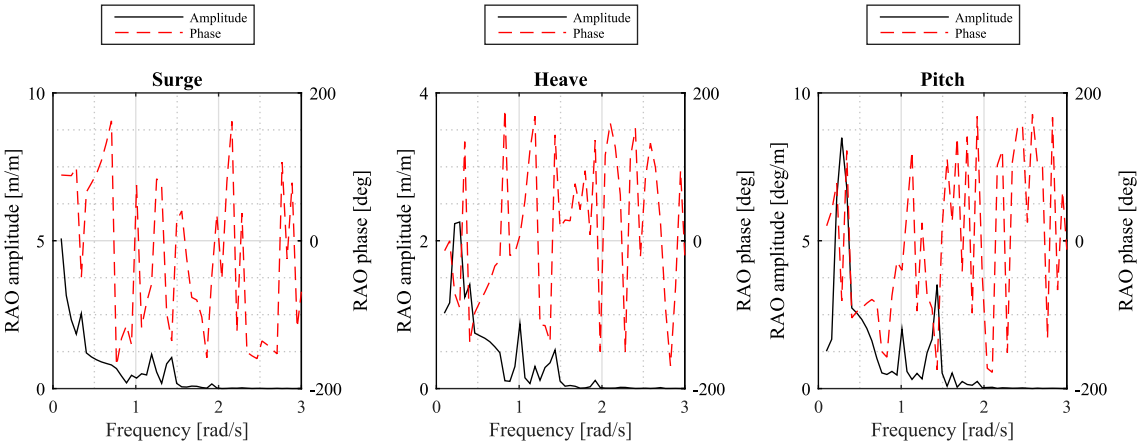

Fig. 5.6. Motion RAO amplitudes and phases for surge, heave and pitch DoF. Note the different y-axes.

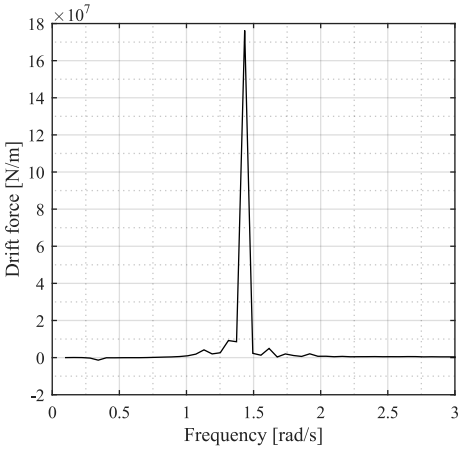

Fig. 5.7. The wave drift coefficients in the surge DoF.

In addition, other studies [15] have suggested to add additional damping according to the values in Table 5.2.

DoF	Additional damping
Surge	$5.39 \cdot 10^5 \ \frac{\text{N}}{\text{m/s}^2}$
Pitch	$6.39 \cdot 10^9 \ \frac{\text{N m}}{\text{rad/s}}$

Table 5.2. Additional damping suggested by [15] to include in numerical time domain models of the Wave Dragon.

5.4 Drag Element Approximations

In order to account for drag loads and quadratic damping, a drag element should be added to the numerical model according to [6]. Consequently, drag coefficients and areas need to be defined for each DoF. Following the procedure in [6], a simplified model of the Wave Dragon is constructed, using geometrical shapes for which the drag coefficients are known from literature. The simplified geometry is illustrated in Fig. 5.8. The values are defined in Table 5.3 for both the geometry below and above SWL. Thereby, both wind and water loads can be included in the model.

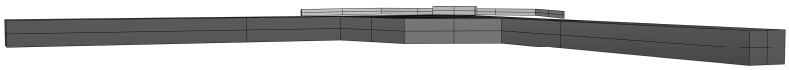

Fig. 5.8. Illustration of the simplified geometry used for calculation of drag coefficients. The dark color resembles the geometry below the SWL, while the light grey color resembles geometry above.

DoF	Drag area	C_d	Load origin (z)
		Below SWL	
Surge	1300 m^2	2.20	-0.9 m
Heave	2651 m^2	1.30	0.0 m
Pitch	$54.17 \cdot 10^6$ m^5	1.30	0.0 m
		Above SWL	
Surge	213 m^2	1.10	4.3 m

Table 5.3. Drag force coefficients and areas for the Wave Dragon.

6 | Comparison of WECs

The four WECs presented in this report are all part of the *"Mooring Solutions for Large Wave Energy Converters"* project, because they are classified as large WECs with passive mooring systems. In addition, they are planned for deployment in similar conditions and hence, it is expected that similar analysis procedure and results can be obtained. In order to illustrate the difference between the devices, Fig. 6.1 illustrates the difference in the geometrical dimensions.

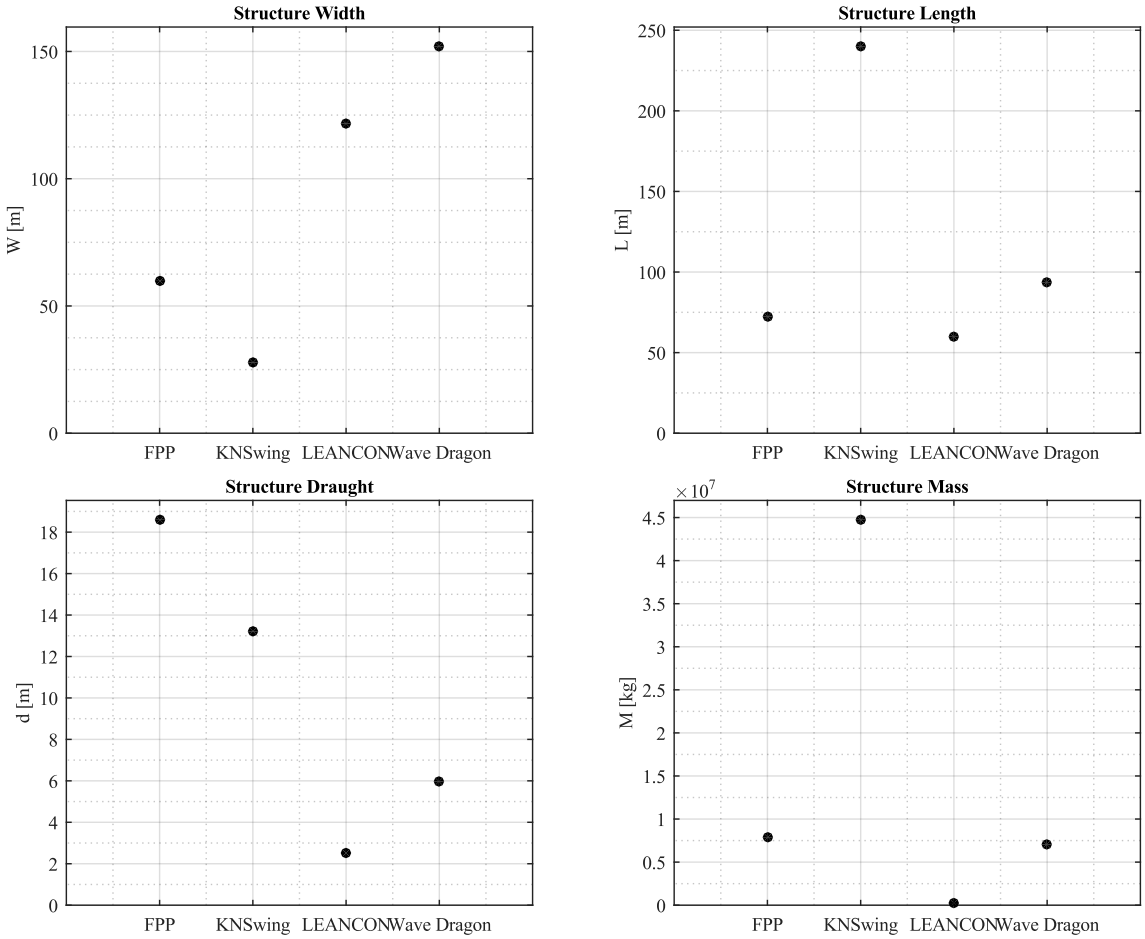

Fig. 6.1. Comparison of geometries of the four WECs presented in this report.

Similarly, Fig. 6.2-6.6 compare the hydrodynamic coefficients for the devices.

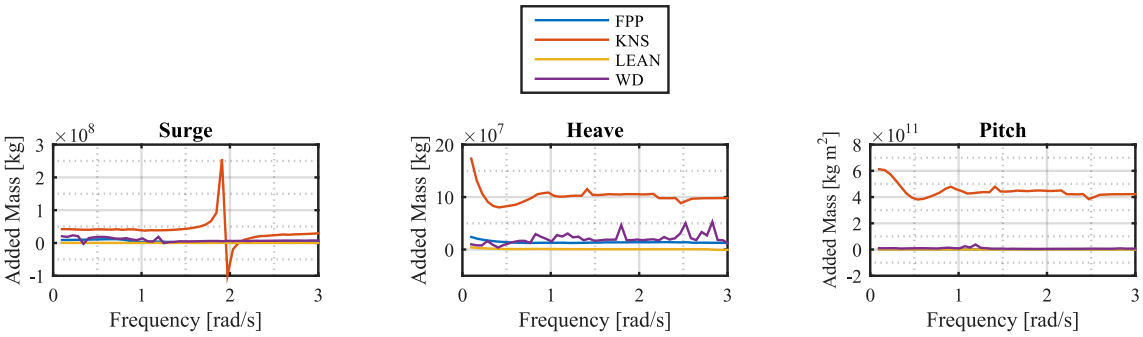

Fig. 6.2. Comparison of added mass coefficients for the four investigated WECs.

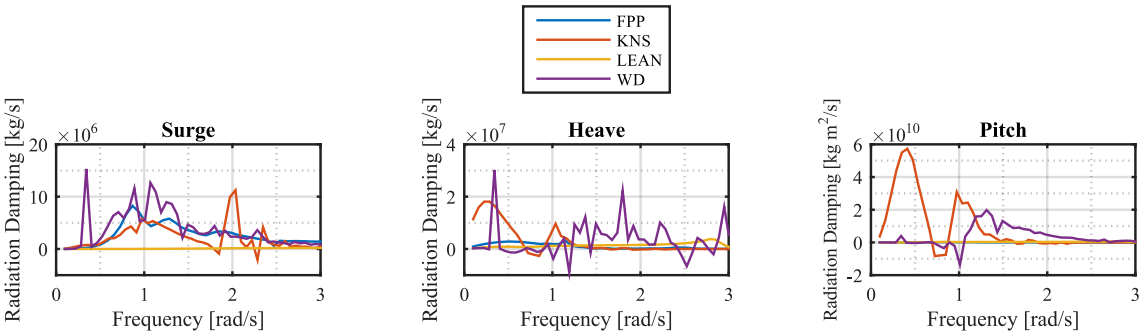

Fig. 6.3. Comparison of radiation damping coefficients for the four investigated WECs.

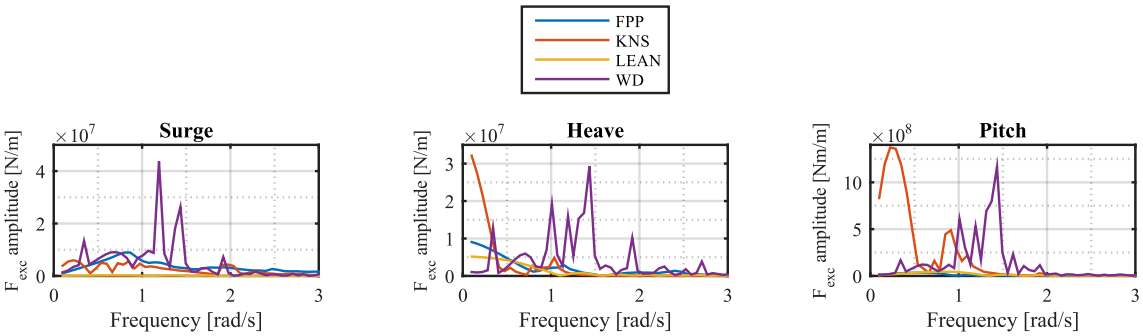

Fig. 6.4. Comparison of wave excitation force coefficients for the four investigated WECs.

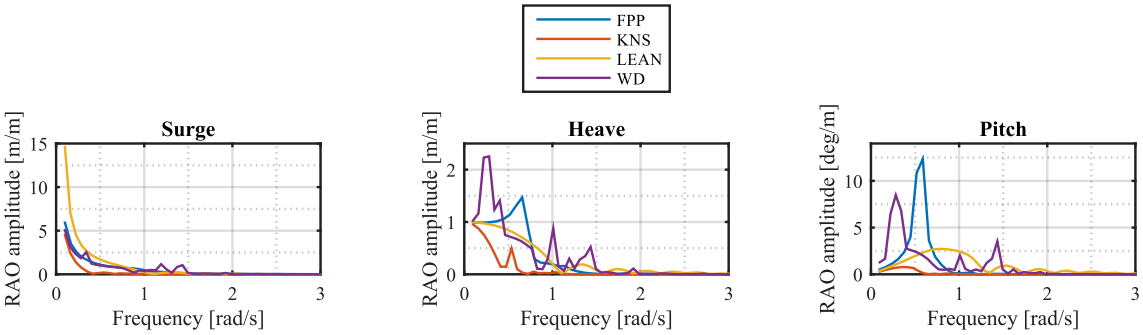

Fig. 6.5. Comparison of motion RAOs for the four investigated WECs.

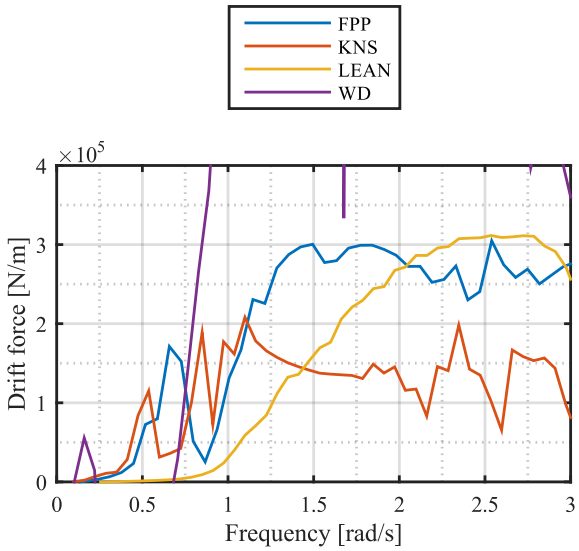

Fig. 6.6. Comparison of wave drift coefficients for the four investigated WECs.

It is evident that despite all being large floating WECs, some differences must be expected in the load and motion response of the devices. Particularly the Wave Dragon will see a significant response in a dynamic analysis compared to the rest of the devices, as it is seen to experience much larger load and motions, especially drift loads. As mention in a previous chapter, this is still a result of inaccurate results from the use of BEM when considering an overtopping device.

Bibliography

[1] Aurélien Babarit and Gérard Delhommeau. Theoretical and numerical aspects of the open source bem solver nemoh. In *11th European Wave and Tidal Energy Conference (EWTEC2015)*, 2015.

[2] Jonas Bjerg Thomsen, Francesco Ferri, Jens Peter Kofoed, and Kevin Black. Cost optimization of mooring solutions for large floating wave energy converters. *Energies*, 11(1), 2018. The article is published in a Special Issue of Energies, "Wave Energy Potential, Behavior and Extraction".

[3] Arthur Francois Serge Pecher and Jens Peter Kofoed. *Handbook of Ocean Wave Energy*, volume 7. Springer, Germany, 2017. This book is open access under a CC BY-NC 2.5 license.

[4] Jonas Bjerg Thomsen, Francesco Ferri, and Jens Peter Kofoed. *Current Mooring Design in Partner WECs and Candidates for Preliminary Analysis: CM1 & M3.* Aalborg University, Department of Civil Engineering, 2016. Confidential report.

[5] Jonas Bjerg Thomsen, Jens Peter Kofoed, Martin Delaney, and Stephen Banfield. Initial Assessment of Mooring Solutions for Floating Wave Energy Converters. In *The 26th International Ocean and Polar Engineering Conference ISOPE2016.* International Society of Offshore and Polar Engineers, 2016.

[6] Jonas Bjerg Thomsen, Francesco Ferri, and Jens Peter Kofoed. Validation of a Tool for the Initial Dynamic Design of Mooring Systems for Large Floating Wave Energy Converters. *Journal of Marine Science and Engineering*, 5(4), 2017.

[7] Jonas Bjerg Thomsen, Francesco Ferri, and Jens Peter Kofoed. Experimental Testing of Moorings for Large Floating Wave Energy Converters. *Progress in Renewable Energies Offshore RENEW2016*, 2016.

[8] Jonas Bjerg Thomsen, Francesco Ferri, and Jens Peter Kofoed. *Experimental Testing and Validation of Selected Tools for Mooring Analysis: M5, T4.1 & T4.2.* Department of Civil Engineering, Aalborg University, 2018.

[9] Subrata Kumar Chakrabarti. *Hydrodynamics of offshore structures.* WIT press, 1987.

[10] JR Morison, JW Johnson, SA Schaaf, et al. The force exerted by surface waves on piles. *Journal of Petroleum Technology*, 2(05):149–154, 1950.

[11] Harry B Bingham, Damien Ducasse, Kim Nielsen, and Robert Read. Hydrodynamic analysis of oscillating water column wave energy devices. *Journal of Ocean Engineering and Marine Energy*, 1(4):405–419, 2015.

[12] Chang-Ho Lee. *WAMIT theory manual.* Massachusetts Institute of Technology, Department of Ocean Engineering, 1995.

[13] DNV. *DNV-OS-E301: Position Mooring*. DNV Offshore Standards, 2010.

[14] Orcina Ltd. *Orcaflex User Manual*. 2013.

[15] Stefano Parmeggiani. *Design of the Wave Dragon Mooring System: setup of a numerical model for time-domain analysis*. Department of Civil Engineering, Aalborg University, Denmark, 2013.

ISSN 1901-726X
DCE Technical Report No. 246